

Azimuthal collimation of long range rapidity correlations by strong color fields in high multiplicity hadron-hadron collisions

Kevin Dusling¹ and Raju Venugopalan²

¹*Physics Department, North Carolina State University, Raleigh, NC 27695, USA*

²*Physics Department, Brookhaven National Laboratory, Upton, NY 11973, USA*

The azimuthal collimation of di-hadrons with large rapidity separations in high multiplicity p+p collisions at the LHC is described in the Color Glass Condensate (CGC) effective theory [1] by N_c^2 suppressed multi-ladder QCD diagrams that are enhanced α_S^{-8} due to gluon saturation in hadron wavefunctions. We show that quantitative computations in the CGC framework are in good agreement with data from the CMS experiment on per trigger di-hadron yields and predict further systematics of these yields with varying trigger p_T and charged hadron multiplicity. Radial flow generated by re-scattering is strongly limited by the structure of the p+p di-hadron correlations. In contrast, radial flow explains the systematics of identical measurements in heavy ion collisions.

The discovery of di-hadron correlations in high multiplicity proton-proton collisions [2], long range in the angular (pseudo-rapidity) separation of the pairs relative to the beam axis and collimated in their relative azimuthal angle about this axis, provides significant insight into rare parton configurations in the proton and their dynamics in hadronic collisions.

High multiplicity proton-proton collisions select “hot spot” configurations of wee gluon states in each proton. Quantum Chromodynamics (QCD) predicts that such hot spots have a maximum occupancy of order α_S^{-1} [3, 4] (α_S being the QCD fine structure constant), and have a typical size $\sim 1/Q_S$, where Q_S is a dynamical saturation scale. This scale grows with the energy and centrality of the collision; when $Q_S \gg \Lambda_{\text{QCD}}$, the fundamental QCD scale, highly occupied hadron wavefunctions can be described using weak coupling methods.

A weak coupling effective field theory (EFT) that describes high density wee parton configurations in the proton is the Color Glass Condensate (CGC) [5]. When CGC’s shatter in a high multiplicity collision, multiparticle production is a consequence of approximately boost invariant radiation from “Glasma flux tubes” of transverse size $1/Q_S$ [6]. Multiplicity distributions [7] derived from factorization theorems [8] in this framework are in good agreement [9, 10] with recent LHC data [11]. Long range rapidity correlations of gluons computed in the CGC EFT [12] were previously shown to be in qualitative agreement [1] with the CMS di-hadron correlation data.

A source of long range rapidity correlations in hadron-hadron collisions are back-to-back gluons emitted from a single t -channel gluon ladder; another source, called “Glasma graphs” are gluons emitted from two separate ladders. Representative graphs of each are shown in fig. (1). In the “dilute” high p_T perturbative limit of QCD, the back-to-back contribution is dominant. However, at high parton densities, when $Q_S^2 \gg \Lambda_{\text{QCD}}^2$, and $p_T^2 \sim Q_S^2$, the effective coupling of gluons in ladders to strong color sources at higher rapidities changes from

$g \rightarrow 1/g$. This corresponds to an enhancement of Glasma graphs by α_S^{-8} compared to the α_S^{-4} enhancement of the back-to-back graphs. Equally important are the very different azimuthal structures of the two long range rapidity correlations. Back-to-back graphs, as the name suggests, are kinematically constrained to be peaked “away side” at relative azimuthal angle $\Delta\phi \sim \pi$ and have a negligible “near side” collimation at $\Delta\phi \sim 0$ as seen in high energy asymptotics that produce a long range rapidity correlation [13, 14].

In contrast, Glasma graphs give identical near and away side contributions because gluon emission is from independent ladders. As also noticed elsewhere [15, 16], these correlated contributions producing an azimuthal collimation are of order $1/N_c^2$; their contribution would be negligible if one did not have the α_S^{-8} enhancement in the high multiplicity region. Within the CGC framework itself, there are leading N_c correlated multi-ladder contributions [8] which are long range in rapidity. However, these do not produce an azimuthal collimation [17, 18]. Likewise, there can be pomeron loop effects outside the framework of ref. [8]; again, these either do not give a collimation or the collimation vanishes rapidly with increasing rapidity [19, 20]. However, a Zero-Yield-at Minimum (ZYAM) procedure [21] used by the CMS collaboration to compute the per trigger near side di-hadron yield [22] only measures contributions that are collimated in $\Delta\phi$ above the $\Delta\phi$ -independent background. The ZYAM procedure allow one to focus on those di-hadron correlations that produced a collimated near side yield. This is also fortuitous because the relative normalization between Glasma graphs and back-to-back graphs necessary to reproduce the di-hadron yield in the entire $\Delta\Phi$ range is not under theoretical control.

The correlated two gluon glasma distribution, expressed in terms of the two particle momentum space rapidities $y_{p,q}$ and transverse momenta p_\perp, q_\perp , is [12]

$$\frac{d^2 N_{\text{Glasma}}^{\text{corr.}}}{d^2 \mathbf{p}_T d^2 \mathbf{q}_T dy_p dy_q} = \frac{C_2}{\mathbf{p}_T^2 \mathbf{q}_T^2} \int_{\mathbf{k}_T} (D_1 + D_2), \quad (1)$$

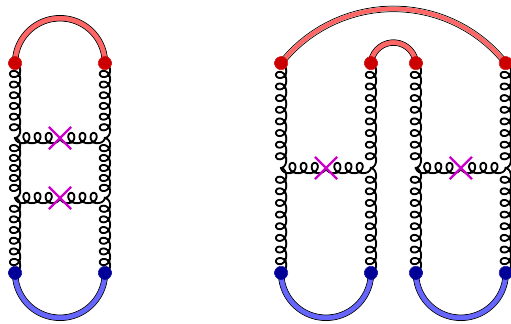


FIG. 1. Representative back-to-back (left) and Glasma graphs (right) in perturbative QCD.

where [23] $C_2 = \frac{\alpha_s^2}{4\pi^{10}} \frac{N_C^2 S_\perp}{(N_C^2 - 1)^3 \zeta}$ and

$$\begin{aligned} D_1 &= \Phi_{A_1}^2(y_p, \mathbf{k}_T) \Phi_{A_2}(y_p, \mathbf{p}_T - \mathbf{k}_T) D_{A_2} \\ D_2 &= \Phi_{A_2}^2(y_q, \mathbf{k}_T) \Phi_{A_1}(y_p, \mathbf{p}_T - \mathbf{k}_T) D_{A_1}, \end{aligned} \quad (2)$$

with $D_{A_{2(1)}} = \Phi_{A_{2(1)}}(y_q, \mathbf{q}_T + \mathbf{k}_T) + \Phi_{A_{2(1)}}(y_q, \mathbf{q}_T - \mathbf{k}_T)$. For our computation, we will also need the single inclusive gluon distribution

$$\frac{dN_1}{dy_p d^2\mathbf{p}_T} = \frac{C_1}{\mathbf{p}_T^2} \int_{\mathbf{k}_T} \Phi_{A_1}(y_p, \mathbf{k}_T) \Phi_{A_2}(y_p, \mathbf{p}_T - \mathbf{k}_T), \quad (3)$$

with the coefficient $C_1 = \frac{\alpha_s N_C S_\perp}{4\pi^6 (N_C^2 - 1)}$. The important ingredient in these expressions is the unintegrated gluon distribution (UGD) per unit transverse area, defined as

$$\Phi_A(y, k_\perp) = \frac{\pi N_C k_\perp^2}{2\alpha_S} \int_0^\infty dr_\perp r_\perp J_0(k_\perp r_\perp) [1 - \mathcal{T}_A(y, r_\perp)]^2 \quad (4)$$

Here \mathcal{T}_A is the forward scattering amplitude of a quark-antiquark dipole of transverse size r_\perp on the target A ; it, or equivalently, the UGD, is a universal quantity that can be determined by solving the Balitsky-Kovchegov (BK) equation [24, 25] as a function of the rapidity $y = \log(x_0/x)$. Solutions of the running coupling BK (rcBK) equation [26] used to compute structure functions are in good agreement with the HERA inclusive data [27].

The eqs. (1) and (3) are obtained from the CGC formalism in ref. [8] for collisions of high high parton density sources, as may be realized in nucleus-nucleus and high multiplicity proton-proton collisions. We emphasize that, albeit not shown explicitly in fig. (1), the derivation of eq. (1) in ref. [12] encodes the effect of radiation between the sources and the triggered gluons as well as the radiation between the gluons. In obtaining these results, the distribution of color sources is assumed to be a non-local Gaussian distribution, whose variance is simply related to $\Phi_A(y, k_\perp)$. This assumed distribution has been shown recently to provide a good approximate solution to the Balitsky-JIMWLK hierarchy for n -point light-like Wilson line correlators [28, 29]. The unintegrated

gluon distribution in eq. (4) have a “bell-shaped” structure peaked at Q_S , with the peak moving to larger k_\perp with increasing rapidity. Thus eqs. (1) and (3) are infrared finite unlike the expressions in ref. [7]. However, like the latter, they do not include multiple scattering contributions that are present in the formalism of ref. [8] and contribute for $k_\perp \leq Q_S$. Their effect on eq. (1) is given by a non-perturbative constant [30] ζ estimated numerically in ref. [31] to be in the range 1/3–3/2. Fits to p+p multiplicity distributions for a range of energies at the LHC and A+A multiplicity distributions at RHIC obtained $\zeta = 1/6$ [9, 10]. Given uncertainties in the numerical computation we will use the latter empirical value instead.

Qualitatively, the origin of a large collimated contribution from Glasma graphs occurs because the integrand in eq. (1) is large when the peaks of the “bell-shaped” unintegrated distributions strongly overlap, $|\mathbf{k}_T| \sim |\mathbf{p}_T - \mathbf{k}_T| \sim |\mathbf{q}_T \pm \mathbf{k}_T| \sim Q_S$, giving a collimation at $\Delta\Phi = 0, \pi$. In practice, the result is smeared by fragmentation effects as well as the details of the integration. We will therefore in the rest of this letter focus on the quantitative contribution of the Glasma graphs and compare the systematics to the CMS proton-proton collision data. We will also explore the relative role of radial flow in generating near side yields in proton-proton and nucleus-nucleus collisions.

The initial condition in rcBK is the McLerran-Venugopalan-like (MV)- initial condition [32] for \mathcal{T}_A at the initial rapidity (corresponding to Bjorken $x \equiv x_0 = 0.01$). The minimum bias saturation scale Q_0^2 in the MV initial condition at the initial rapidity and the transverse area S_\perp are adjusted to reproduce the single inclusive p+p distribution in eq. (3)–for a more detailed discussion, see ref. [9]. Diffractive scattering results from HERA indicate a strong dependence of the saturation scale on impact parameter or the centrality of the collision [33]. The centrality dependence of eq. (4) is therefore studied here by keeping S_\perp fixed and varying Q_0^2 at the initial rapidity scale [34]. We follow the results of the HERA studies in ref. [33] and choose Q_0^2 values in the fundamental representation of 0.15, 0.3, 0.45 and 0.6 GeV^2 to represent different centralities in computing the di-hadron yield [35].

Further calculational details are as follows. The strong coupling constant, α_S , is evaluated at the saturation scale. Because the di-hadrons of interest are widely separated in rapidity, we assume that gluons fragment independently. Fragmentation functions at forward rapidities are not particularly well known [36]; these will be better constrained as more data from the LHC becomes available. For our purposes, we consider a soft fragmentation function $D_1(x) = 3(1-x)^2/x$ and a hard one $D_2(x) = 2(1-x)/x$; the former is closer to the NLO fit function for gluon fragmentation to pions [37], while the latter allows for hadrons to carry on average a larger frac-

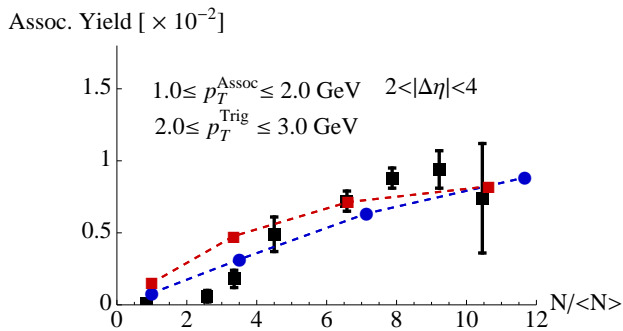


FIG. 2. Associated yield for four different initial saturation scales representing different centralities. The blue circles (red squares) represent the softer (harder) $D_1(z)$ ($D_2(z)$) fragmentation functions. Dashed lines connect computed points to guide the eye. Data points are from the CMS collaboration [21].

tion of the gluon momentum. Finally, we introduce an overall constant K factor which is the only parameter fit to the data presented here. It accounts for higher order corrections (both in our framework as well as in the fragmentation functions) in addition to corrections necessary to fully implement the experimental acceptance [38].

For our analysis of the CMS data, we define

$$N_{\text{trig}} = \int_{-2.4}^{+2.4} d\eta \int_{p_T^{\text{min}}}^{p_T^{\text{max}}} d^2 \mathbf{p}_T \int_0^1 dz \frac{D(z)}{z^2} \frac{dN}{d\eta d^2 \mathbf{p}_T} \left(\frac{p_T}{z} \right) \quad (5)$$

and

$$\begin{aligned} \frac{d^2 N}{d\Delta\phi} &= K \int_{-2.4}^{+2.4} d\eta_p d\eta_q \mathcal{A}(\eta_p, \eta_q) \quad (6) \\ &\times \int_{p_T^{\text{min}}}^{p_T^{\text{max}}} \frac{dp_T^2}{2} \int_{q_T^{\text{min}}}^{q_T^{\text{max}}} \frac{dq_T^2}{2} \int d\phi_p \int d\phi_q \delta(\phi_p - \phi_q - \Delta\phi) \\ &\times \int_0^1 dz_1 dz_2 \frac{D(z_1)}{z_1^2} \frac{D(z_2)}{z_2^2} \frac{d^2 N_{\text{Glasma}}^{\text{corr.}}}{d^2 \mathbf{p}_T d^2 \mathbf{q}_T d\eta_p d\eta_q} \left(\frac{p_T}{z_1}, \frac{q_T}{z_2}, \Delta\phi \right) \end{aligned}$$

Here $p_T^{\text{min(max)}}$ and $q_T^{\text{min(max)}}$ refer to bounds on the range of the trigger and associated hadron momenta respectively. Likewise, $\Delta\eta_{\text{min}}(\Delta\eta_{\text{max}}) = 2.0(4.0)$ denote the pseudo-rapidity gap [39] of hadrons within the experimental acceptance $\mathcal{A}(\eta_p, \eta_q) \equiv \theta(|\eta_p - \eta_q| - \Delta\eta_{\text{min}}) \theta(\Delta\eta_{\text{max}} - |\eta_p - \eta_q|)$.

The strength of the correlation in $\Delta\phi$ is quantified by the associated yield computed using the ZYAM procedure defined to be

$$\text{Assoc. Yield} = \frac{1}{N_{\text{trig}}} \int_0^{\Delta\phi_{\text{min.}}} d\Delta\phi \frac{d^2 N}{d\Delta\phi} - \left. \frac{d^2 N}{d\Delta\phi} \right|_{\Delta\phi_{\text{min.}}} \quad (7)$$

where $\Delta\phi_{\text{min.}}$ is the angle at which the two particle correlation strength is minimal. In fig. (2), we plot the associated yield as a function of charged particle multiplicity, per minimum bias multiplicity, for the stated windows in

$\Delta\eta$ and in the associated and trigger particle transverse momenta. As noted previously, the charged particle multiplicity is varied by changing Q_0^2 in the initial conditions for rcBK evolution. We see that the agreement is quite good, especially at the highest multiplicities where we expect our formalism to perform best. At lower multiplicities, the effect of high order corrections as well as impact parameter fluctuations become more important.

In fig. (3), we plot the associated yield versus the p_T trigger window for three associated particle windows as labeled. The top figure corresponding to $1.0 \leq p_T^{\text{Assoc}} \leq 2.0$ GeV also shows the recent CMS measurements of the same quantity. Even though the overall normalization of our calculation needed to be augmented by a constant K -factor, $K = 2.3$, the momentum dependence of our results is parameter free. The other two plots are absolute predictions; though, as shown, they are quite sensitive to fragmentation. The sensitivity of the associated yield to different momentum cuts in our calculation stems from an intrinsic scale (the saturation momentum) where the initial state wave-function is peaked. As argued in [1] maximal angular correlations occur when $|\mathbf{p}_T| \sim |\mathbf{q}_T| \sim Q_S$ and when \mathbf{p}_T and \mathbf{q}_T are parallel. This signal persists after including fragmentation and shows good agreement with the measured high multiplicity pp data. Our model computation provides strong support to the qualitative idea that a significant near side angular correlation at semi-hard trigger and associate hadron momenta of 2–4 GeV is evidence of saturation dynamics.

Because the number of particles produced in the highest multiplicity pp collisions are comparable to those in $Cu Cu$ collisions one may speculate that (above and beyond the collimation provided by our intrinsic QCD effect) collective flow contributes significantly to the angular correlation [40, 41]. To test this hypothesis, we employ a radial boost model where the angular distribution in $\Delta\phi$ in the laboratory frame is related to the corresponding distribution in $\Delta\tilde{\phi}$ in the local rest frame,

$$\frac{d^2 N}{d\Delta\phi} = \int_{-\pi}^{\pi} d\Psi \mathcal{J}(\Psi, \Delta\phi) \frac{d^2 N}{d\Delta\tilde{\phi}} \left(\Delta\tilde{\phi}(\Psi, \Delta\phi) \right), \quad (8)$$

where \mathcal{J} is the Jacobian [42] relating distributions in the two frames. As transverse flow further collimates the signal, the overall strength of the associated yield will increase. However, the momentum dependence changes as well. The effect of the boost is demonstrated in fig. (4). Starting with our correlation in the local rest frame (bottom), we show the result after transverse boosts of (bottom to top) $\beta = 0.1, 0.2, 0.25, 0.3$. One notices a qualitative change in the shape of the associated yield versus p_T^{trig} . For smaller transverse boosts the dependence on p_T^{trig} is given by the intrinsic angular correlation generated by the Glasma graph of fig. (1). For large boost velocities the associated yield is driven by the collimation of the $\Delta\phi$ independent pedestal computed from the same

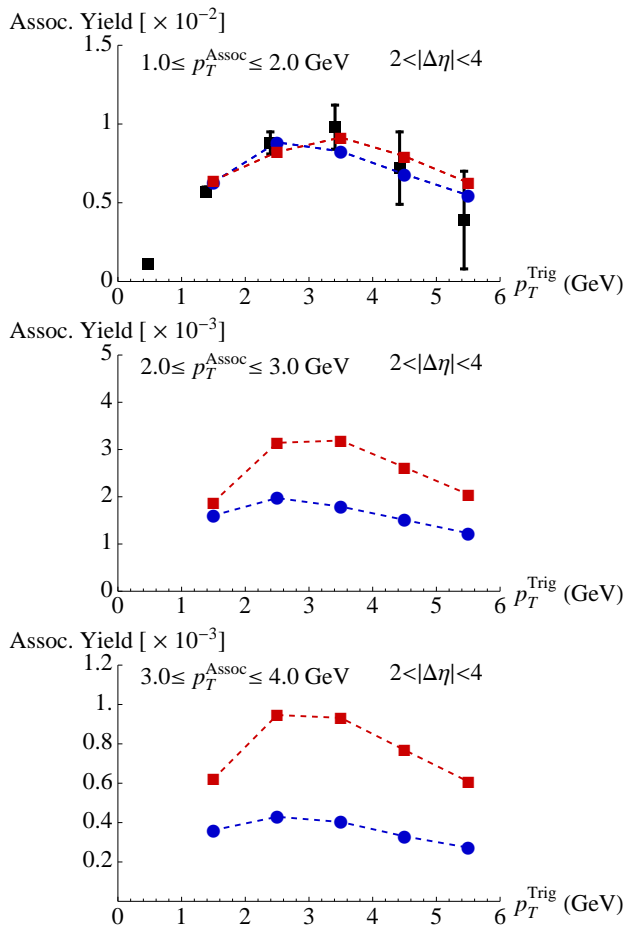


FIG. 3. Associated yield for central $p+p$ ($Q_0^2 = 0.6 \text{ GeV}^2$) collisions using soft (hard) $D_1(z)$ -blue circles ($D_2(z)$ -red squares) fragmentation functions. Dashed lines connect computed points to guide the eye. The black squares are the available CMS data [21] for the $N \geq 110$ multiplicity bin of pp collisions at $\sqrt{s} = 7 \text{ TeV}$. The middle and bottom figures are predictions for the labeled associated p_T windows.

graph. Without any transverse flow this pedestal (or underlying event) is removed by the ZYAM procedure and therefore does not contribute to the associated yield. But after collimation, its signal exceeds that of the intrinsic angular correlation. The change in shape therefore suggests an upper bound of $\beta = 0.25$ in this simple model of flow in pp collisions.

This is in complete contrast to heavy ion collisions where we expect flow to dominate the angular correlation [6, 43, 44]. We demonstrate this with a comparison of the p_T^{trig} dependence of the (collimated by flow) pedestal in the Glasma with data from $Pb Pb$ collisions at $\sqrt{s} = 2.76 \text{ TeV}$ in fig. (5). The agreement is quite good considering the very simple model of radial flow considered here. Flow effects here completely dwarf the intrinsic QCD correlations that were the dominant effect generating the near side azimuthal collimation in pp collisions. We should stress however that the pedestal (while

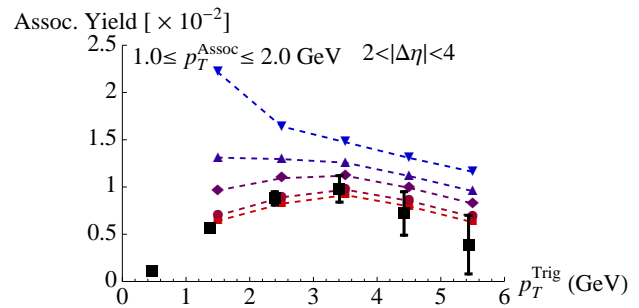


FIG. 4. Effect of transverse flow on the intrinsic pp correlation using the hard $D_2(z)$ fragmentation function. Boosts from bottom to top: $\beta = 0, 0.1, 0.2, 0.25, 0.3$.

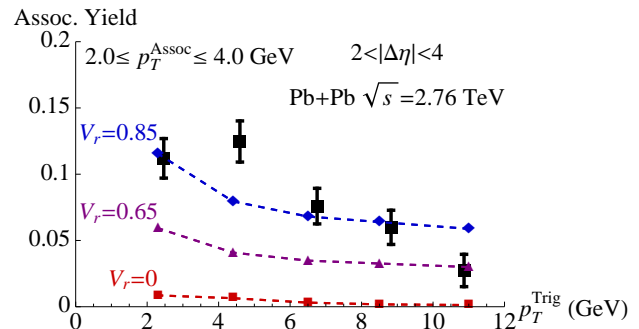


FIG. 5. Computations of the associated per trigger yield in $Pb Pb$ collisions at $\sqrt{s} = 2.76 \text{ TeV}$ using $Q_0^2 = 0.9 \text{ GeV}^2$ in the fundamental representation compared to the CMS data [21]. The curves shown, with the $D_2(z)$ fragmentation function, are for transverse boosts of $\beta = 0, 0.65, 0.85$. At large flow velocities, the intrinsic angular correlation is entirely washed out.

independent of $\Delta\phi$ in the local rest frame) is also an intrinsic two-particle correlation generated by the Glasma graph and the p_T^{trig} dependence seen in fig. (5) is representative of this underlying dynamics.

ACKNOWLEDGEMENTS

We thank Wei Li for helpful clarifications regarding the CMS results. K.D. and R.V. are supported by the US Department of Energy under DOE Contract Nos. DE-FG02-03ER41260 and DE-AC02-98CH10886 respectively.

-
- [1] A. Dumitru, K. Dusling, F. Gelis, J. Jalilian-Marian, T. Lappi, *et al.*, Phys.Lett. **B697**, 21 (2011), arXiv:1009.5295 [hep-ph]
 - [2] V. Khachatryan *et al.* (CMS Collaboration), JHEP **1009**, 091 (2010), arXiv:1009.4122 [hep-ex]

- [3] L. Gribov, E. Levin, and M. Ryskin, Phys.Rept. **100**, 1 (1983)
- [4] A. H. Mueller and J.-w. Qiu, Nucl.Phys. **B268**, 427 (1986)
- [5] F. Gelis, E. Iancu, J. Jalilian-Marian, and R. Venugopalan, Ann.Rev.Nucl.Part.Sci. **60**, 463 (2010), arXiv:1002.0333 [hep-ph]
- [6] A. Dumitru, F. Gelis, L. McLerran, and R. Venugopalan, Nucl.Phys. **A810**, 91 (2008), arXiv:0804.3858 [hep-ph]
- [7] F. Gelis, T. Lappi, and L. McLerran, Nucl.Phys. **A828**, 149 (2009), arXiv:0905.3234 [hep-ph]
- [8] F. Gelis, T. Lappi, and R. Venugopalan, Phys.Rev. **D78**, 054019 (2008), Phys.Rev. **D78**, 054020 (2008), Phys.Rev. **D79**, 094017 (2009).
- [9] P. Tribedy and R. Venugopalan, Nucl.Phys. **A850**, 136 (2011), arXiv:1011.1895 [hep-ph]
- [10] P. Tribedy and R. Venugopalan(2011), arXiv:1112.2445 [hep-ph]
- [11] V. Khachatryan *et al.* (CMS Collaboration), JHEP **1101**, 079 (2011), arXiv:1011.5531 [hep-ex]
- [12] K. Dusling, F. Gelis, T. Lappi, and R. Venugopalan, Nucl.Phys. **A836**, 159 (2010), arXiv:0911.2720 [hep-ph]
- [13] A. Leonidov and D. Ostrovsky, Phys. Rev. **D62**, 094009 (2000), arXiv:hep-ph/9905496
- [14] V. S. Fadin, M. Kotsky, and L. Lipatov(1996), arXiv:hep-ph/9704267 [hep-ph]
- [15] J. Bartels and M. Ryskin(2011), arXiv:1105.1638 [hep-ph]
- [16] E. Levin and A. H. Rezaeian, Phys.Rev. **D84**, 034031 (2011), arXiv:1105.3275 [hep-ph]
- [17] A. Dumitru and J. Jalilian-Marian, Phys.Rev. **D81**, 094015 (2010), arXiv:1001.4820 [hep-ph]
- [18] A. Dumitru, J. Jalilian-Marian, and E. Petreska, Phys.Rev. **D84**, 014018 (2011), arXiv:1105.4155 [hep-ph]
- [19] A. Kovner and M. Lublinsky, Phys.Rev. **D83**, 034017 (2011), arXiv:1012.3398 [hep-ph]
- [20] A. Kovner and M. Lublinsky(2011), arXiv:1109.0347 [hep-ph]
- [21] CMS-PAS-HIN-11-006(2011), <http://cdsweb.cern.ch/record/1353583>
- [22] W. Li (CMS collaboration), J.Phys.G **G38**, 124027 (2011), arXiv:1107.2452 [nucl-ex]
- [23] This prefactor corrects for a typo and is hence a factor of 4 larger than in refs. [1, 12] but in agreement in the appropriate limit with the corresponding expression in ref. [7].
- [24] I. Balitsky, Nucl.Phys. **B463**, 99 (1996), arXiv:hep-ph/9509348 [hep-ph]
- [25] Y. V. Kovchegov, Phys.Rev. **D60**, 034008 (1999), arXiv:hep-ph/9901281 [hep-ph]
- [26] The BK equation is valid at large N_c for dense color sources as a limit of the Balitsky-JIMWLK hierarchy [5]. The finite N_c corrections are however at most $1/N_c^2$; in practice, corrections to the evolution are less than a percent [28, 45].
- [27] J. L. Albacete, N. Armesto, J. G. Milhano, and C. A. Salgado, Phys.Rev. **D80**, 034031 (2009), arXiv:0902.1112 [hep-ph]
- [28] A. Dumitru, J. Jalilian-Marian, T. Lappi, B. Schenke, and R. Venugopalan, Phys.Lett. **B706**, 219 (2011), arXiv:1108.4764 [hep-ph]
- [29] E. Iancu and D. Triantafyllopoulos(2011), arXiv:1112.1104 [hep-ph]
- [30] Multiple scattering effects will quantitatively affect but not qualitatively alter the ϕ distributions in the infrared. Note also, to avoid confusion, ζ here plays the same role as the constant κ in ref. [7].
- [31] T. Lappi, S. Srednyak, and R. Venugopalan, JHEP **1001**, 066 (2010), arXiv:0911.2068 [hep-ph]
- [32] L. D. McLerran and R. Venugopalan, Phys.Rev. **D49** 2233 (1994), Phys.Rev. **D49** 3352 (1994).
- [33] H. Kowalski, L. Motyka, and G. Watt, Phys.Rev. **D74**, 074016 (2006), arXiv:hep-ph/0606272 [hep-ph]
- [34] Since the di-hadron yields are normalized per trigger, the S_\perp dependence drops out for the quantities studied here.
- [35] These initial values should not be confused with the saturation momentum, defined here as the peak of $\phi(y, k_\perp)$, at the much smaller values of $x\sqrt{s} = p_T e^{\pm y}$ probed in the di-hadron studies here, which span (in the adjoint representation), $Q_s^2(x \sim 10^{-4 \div 5}) \sim 1 - 4 \text{ GeV}^2$ respectively for initial saturation scales used in this work.
- [36] R. Sassot, P. Zurita, and M. Stratmann, Phys.Rev. **D82**, 074011 (2010), arXiv:1008.0540 [hep-ph]
- [37] B. A. Kniehl, G. Kramer, and B. Potter, Nucl. Phys. **B582**, 514 (2000), arXiv:hep-ph/0010289
- [38] One example of the latter is N_{trig} , which is required experimentally to be ≥ 2 . Properly implementing this constraint would require Monte-Carlo simulation and is beyond the scope of this work.
- [39] We replace the rapidity y with the pseudo-rapidity η which is a good approximation for the p_T, q_T of interest.
- [40] P. Bozek, Eur.Phys.J. **C71**, 1530 (2011), arXiv:1010.0405 [hep-ph]
- [41] K. Werner, I. Karpenko, and T. Pierog, Phys.Rev.Lett. **106**, 122004 (2011), arXiv:1011.0375 [hep-ph]
- [42] The relationship between the opening angles $\Delta\phi$ in the laboratory frame and the opening angle $\Delta\tilde{\phi}$ in the local rest frame under a Lorentz boost having velocity $v = \beta c$ and direction $2\Psi = \phi_p + \phi_q$ is given by
- $$2 \sin^2 \left(\frac{\Delta\tilde{\phi}}{2} \right) = \frac{\sqrt{1 - \beta^2} (1 - \cos(\Delta\phi))}{1 - 2\beta \cos \Psi \cos \left(\frac{\Delta\phi}{2} \right) + \frac{\beta^2}{2} (\cos(\Delta\phi) + \cos(2\Psi))}.$$
- In addition one must include a Jacobian factor
- $$\mathcal{J} = \frac{1 - \beta^2}{(1 - \beta \cos(\Psi + \Delta\phi/2))(1 - \beta \cos(\Psi - \Delta\phi/2))},$$
- when changing between the local rest frame and laboratory distributions.
- [43] S. A. Voloshin, Phys.Lett. **B632**, 490 (2006), arXiv:nucl-th/0312065 [nucl-th]
- [44] C. A. Pruneau, S. Gavin, and S. A. Voloshin, Nucl.Phys. **A802**, 107 (2008), arXiv:0711.1991 [nucl-ex]
- [45] K. Rummukainen and H. Weigert, Nucl.Phys. **A739**, 183 (2004), arXiv:hep-ph/0309306 [hep-ph]